CHALMERS

FSI-analysis on vibrations of a slender rod exposed to axial flow

Calculations for nuclear power applications

Master's thesis in Engineering Mathematics and Computational Science

KAJSA BENGTSSON

Department of Applied Mechanics
CHALMERS UNIVERSITY OF TECHNOLOGY
Göteborg, Sweden 2016

MASTER'S THESIS IN ENGINEERING MATHEMATICS AND COMPUTATIONAL SCIENCE

FSI-analysis on vibrations of a slender rod exposed to axial flow

Calculations for nuclear power applications

KAJSA BENGTSSON

Department of Applied Mechanics
Division of Fluid Dynamics
CHALMERS UNIVERSITY OF TECHNOLOGY

Göteborg, Sweden 2016

FSI-analysis on vibrations of a slender rod exposed to axial flow
Calculations for nuclear power applications
KAJSA BENGTSSON

© KAJSA BENGTSSON, 2016

Master's thesis 2016:03
ISSN 1652-8557
Department of Applied Mechanics
Division of Fluid Dynamics
Chalmers University of Technology
SE-412 96 Göteborg
Sweden
Telephone: +46 (0)31-772 1000

Chalmers Reproservice
Göteborg, Sweden 2016

FSI-analysis on vibrations of a slender rod exposed to axial flow
Calculations for nuclear power applications
Master's thesis in Engineering Mathematics and Computational Science
KAJSA BENGTSSON
Department of Applied Mechanics
Division of Fluid Dynamics
Chalmers University of Technology

Abstract

Vibration on components caused by flow, so called flow induced vibrations (FIV), is an important area in many industrial fields. Fluid-structure interaction problems can be solved by coupling a structure solver to a fluid solver and in each time step iterate to a solution. Different solvers can be used, but the coupling codes still need to be tested and evaluated to be used for industrial purposes.

Experiments have been performed to create data for FSI-software validation and to see how an axial flow along a slender structure can cause vibrations of the structure. In order to prove the reliability of the FSI-simulation software the purpose of this master's thesis is to see if the rod vibrations, induced by the axial flow, can be predicted with coupled FSI-simulations in ANSYS. An FSI-analysis of the same geometry as in the experiments has been carried out and the simulation data were compared to the experiment data. Different meshes, different turbulence models and structural damping were also investigated on how they affected the solution.

The LES turbulence model could induce vibrations, while the URANS turbulence model could not. The vibration frequencies match the eigenfrequencies for the tube. The amplitudes increase with increased mass flow. The amplitudes were far too high and the frequencies were a bit higher in the simulations compared to the experiment. The differences could be because of discrepancies between the ANSYS model and the experiment, since there were some uncertainties in the documentation of the experiment. The simulations seemed not to be sensitive to time step or damping, but a coarse mesh resulted in lower amplitudes compared to a finer one.

Keywords: Nuclear power, Fluid Structure Interaction, FSI, CFD, Vibration, FIV, ANSYS Workbench

Preface

This thesis started in February 2015 and completes the master's programme Engineering Mathematics and Computational Science at Chalmers University of Technology in Gothenburg, Sweden. The master's thesis work has been carried out at Onsala Ingenjörsbyrå AB in Kungsbacka and is financed by Energiforsk AB.

Acknowledgements

I would like to acknowledge Onsala Ingenjörsbyrå for providing me with supervisors and computational resources. A special thanks to my supervisors at Onsala, Pascal Veber and Joakim Grundberg, who shared their knowledge and contributed ideas and guidance. I would also like to thank the other people at Onsala who always took their time to help and answer questions. I want to show my gratitude to Energiforsk for financing this master's thesis work. Furthermore, I would like to thank Ansys Sweden for great technical support and especially Tobias Berg for his interest, help and advices. Finally I would like to thank my examiner Lars Davidson who are always helpful and take the time to answer questions.

Kajsa Bengtsson, Kungsbacka, October 2015

Contents

1 Introduction

Vibration on components caused by flow, so called *flow induced vibrations (FIV)*, is an important area in many industrial fields, including the nuclear power as the fuel rod and also other slender structures are affected by the cooling water flow. This is a phenomena where it becomes an interaction between the fluid and the structure as the flow may cause vibrations on the structure due to turbulence, but also the motion of the structure will affect the flow path. *Fluid-structure interaction (FSI)* problems can be solved by coupling a structure solver to a fluid solver and in each time step iterate to a solution. Different solvers can be used, but the coupling codes still need to be tested and evaluated, to be used for industrial purposes. Therefore experimental data is important for benchmarking of FSI-codes.

1.1 Background

Energiforsk AB is a company working with research and development in the energy sector. Energiforsk together with Vattenfall's Research and Development have performed experimental tests on a simplified geometry of the in-core neutron flux detector system guide tubes, located in between the fuel bundles as in Figure 1.1. The length of the guide tube is 4040 mm and the diameter is 19 mm. The cooling water flows axially upwards along the guide tube and the space between the fuel bundles and the tube is less then 15 mm. Since the tube is weak and channel is small, even small displacements of the tube will cause pressure differences in the flow resulting in forces on the tube.

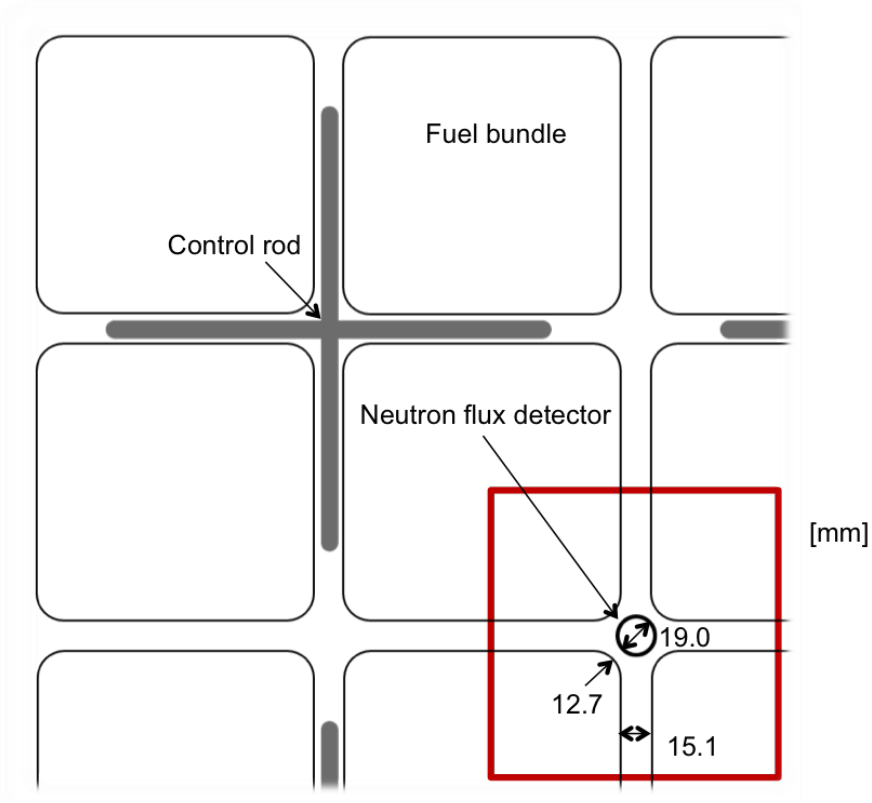

Figure 1.1: *Schematic of the fuel bundles and the neutron flux detectors.*

The tube is fixed in its lower end and fastened in a grid with a spring at its upper end. The domain considered in the experiment is marked in Figure 1.1. The geometry in the experiment is scaled down and the upper boundary condition is a bit simplified, the dimensions and boundary conditions of the experiment geometry are described in section 3.1. At the inlet the mass flow rate varied between zero and 15 kg/s, and the pressure is fixed at the outlet.

The experimental data consists of time history data of the tube displacement and the pressure in the channel between the tube and the walls of the surrounding "fuel bundles", for varying flow velocities. The tube displacement is measured with two high speed cameras located at 90 degree angle to each other, a picture of the rig is shown in Figure A.1 in appendix A. The purpose of the experiment is to create data for FSI-software validation and to see how an axial flow along a slender structure can cause vibrations of the structure.

1.2 Purpose

In order to prove the reliability of the FSI-simulation software the purpose of this master's thesis is to see if the rod vibrations, induced by the axial flow, can be predicted with coupled FSI-simulations in ANSYS.

1.3 Objective

An FSI-analysis of the same geometry as in the experiments will be carried out with ANSYS software, and a working model needs to be set up in ANSYS. The tube displacement data from the simulation will be evaluated with focus on frequency content and magnitude of the amplitudes. The simulation data will be compared to the experiment data. It will also be investigated how different meshes, different turbulence models and structural damping will affect the solution. In ANSYS a *stabilization parameter* is implemented in order to stabilize the solution and avoid divergence. It will be investigated how the stabilization parameter is implemented and how it affect the convergence and the solution.

1.4 Scope

The FSI-analysis will be done only with ANSYS Workbench coupling ANSYS Mechanical with ANSYS Fluent, no other software will be used in this thesis. In the test rig the tube is welded in its lower end in a cross formed structure which also serves as a flow straightener. This part is outside the computational domain and not included in the simulation. The experiments is done for many different inlet mass flow rates, but only three different inlet mass flows will be considered in the simulations, and the sensitivity analyses will be done only for one inlet mass flow.

1.5 Stakeholders

Energiforsk AB finances the experiments and this master's thesis. The experiments are performed by Vattenfall R&D in their research facility in Älvkarleby. This master's thesis will is performed together with and supervised by the people at Onsala Ingenjörsbyrå AB, an

engineer office with focus on computationally intensive structural and fluid calculations. They are specialized in advanced solid and fluid dynamics, and how these phenomena interact. The main part of their work is concentrated to the Swedish nuclear industry. Another master's thesis is performed at KTH Royal Institute of Technology with the same purpose, but using another software (OpenFoam).

2 Theory

In this chapter a theoretical background for understanding the methods and result is given. First some basic theory about the structural model and the fluid model is given. Then different approaches for FSI-analyses are described and a presentation of the ANSYS software is given. For understanding the post processing of the data a brief explanation of the discrete Fourier transform is given.

2.1 Structural model

Almost all physical problems end up with solving a differential equation, which is not always possible to solve analytically. A numerical method for solving these differential equation approximately is called the *Finite Element Method (FEM)*. The structure is split up in small parts, so called finite elements, and the differential equation is solved approximately for each element. The steps in the FE-formulation is to multiply the differential equation with a test function, integrate over the element and use the Green-Gauss theorem to rewrite the equation. Then the unknown function is approximated with $\mathbf{Na}$ where a_i is the nodal value in node i and N_i is a function taking the value one in node i and zero in all other nodes. The result is a discretized system of equations, that gives an approximate solution for the whole structure. [1]

2.1.1 Equation of motion and mode separation

The equation of motion for a discretized multiple degrees of freedom system is given by

$$[\mathrm{M}]\ddot{\mathbf{u}}(t) + [\mathrm{C}]\dot{\mathbf{u}}(t) + [\mathrm{K}]\mathbf{u}(t) = \mathbf{F}(t) \tag{2.1}$$

where $\mathbf{u}(t)$ is the displacement vector, $\mathbf{F}(t)$ is the load vector, [M] is the mass matrix, [C] is the damping matrix and [K] is the stiffness matrix. *Reyleigh damping* is often assumed and modeled as $[\mathrm{C}] = \alpha[\mathrm{M}] + \beta[\mathrm{K}]$. For an undamped system with zero load (2.2) the motions will be on the harmonic form $\mathbf{u}_n(t) = \boldsymbol{\phi}_n \sin(\omega_n t + \varphi)$, when inserted in (2.2) leads to the eigenvalue problem (2.3) where $\boldsymbol{\phi}_n$ is the eigenvector corresponding to eigenvalue ω_n^2.

$$[\mathrm{M}]\ddot{\mathbf{u}}(t) + [\mathrm{K}]\mathbf{u}(t) = \mathbf{0} \tag{2.2}$$

$$([\mathrm{K}] - \omega_n^2[\mathrm{M}])\boldsymbol{\phi}_n = \mathbf{0} \tag{2.3}$$

By superposition the general solution to (2.2) is a linear combination of $\{\mathbf{u}_n\}_{n=1}^N$.

$$\mathbf{u}(t) = \sum_{n=1}^{N} a_n \mathbf{u}_n(t) = \sum_{n=1}^{N} a_n \boldsymbol{\phi}_n \sin(\omega_n t + \varphi) \tag{2.4}$$

The general solution to the damped system (2.1), with Reyleigh damping assumed, can be written in terms of the modes as (2.5) and (2.6).

$$\mathbf{u}(t) = \sum_{n=1}^{N} \mathbf{u}_n = \sum_{n=1}^{N} \boldsymbol{\phi}_n q_n(t) \tag{2.5}$$

$$m_n\ddot{q}_n(t) + c_n\dot{q}_n(t) + k_n q_n(t) = F_n(t) \tag{2.6}$$

where

$$F_n(t) = \boldsymbol{\phi}_n^T \mathbf{F}(t), \quad m_n = \boldsymbol{\phi}_n^T [\mathrm{M}] \boldsymbol{\phi}_n, \quad k_n = \boldsymbol{\phi}_n^T [\mathrm{K}] \boldsymbol{\phi}_n = \omega_n^2 m_n,$$
$$c_n = \boldsymbol{\phi}_n^T [\mathrm{C}] \boldsymbol{\phi}_n = \alpha m_n + \beta k_n = (\alpha + \beta\omega_n^2) m_n$$

Equation (2.3) gives that $k_n = \omega_n^2 m_n$ and hence $c_n = (\alpha + \beta\omega_n^2)m_n$. Equation (2.6) can then be written as

$$\ddot{q}_n(t) + 2\zeta_n\omega_n\dot{q}_n(t) + \omega_n^2 q_n(t) = \frac{F_n(t)}{m_n} \tag{2.7}$$

where $\zeta_n = \alpha/2\omega_n + \beta\omega_n/2$ is the damping ratio for the n:th mode. In simulations only stiffness damping (β) is implemented and calculated as $\beta = 2\zeta/\omega$ where ζ and ω is estimated from experiments. [2]

2.1.2 Derivation of nodal positions for a fixed-pinned beam

The differential equation for bending vibration of a homogenous beam with length L is given by (2.8) [3].

$$EI\frac{\partial^4 w}{\partial x^4} + \rho A_0 \frac{\partial^2 w}{\partial t^2} = 0 \tag{2.8}$$

Assuming the solution is on the form $w(x,t) = X(x)T(t)$ equation (2.8) can be written as

$$\frac{X^{(4)}(x)}{X(x)} = -\frac{\rho A_0}{EI}\frac{T''(t)}{T(t)} = \lambda. \tag{2.9}$$

Since the left hand side is independent of t and right hand side is independent of x both sides must be constant. This gives, after some rearranging, equation (2.10).

$$X^{(4)}(x) - \mu^4 X(x) = 0, \quad \mu^4 = \lambda \tag{2.10}$$

Solving equation (2.10) for the fixed-pinned boundary condition gives solutions on the following form

$$\begin{aligned} X_n(x) = c_n\big((\sin\mu_n L + \sinh\mu_n L)(\cos\mu_n x - \cosh\mu_n x) \\ -(\cos\mu_n L + \cosh\mu_n L)(\sin\mu_n x - \sinh\mu_n x)\big) \end{aligned} \tag{2.11}$$

where $(\mu_n L)$ is roots to equation (2.12), which must be satisfied for the equation (2.10) to have other solutions than the trivial.

$$\cos x \sinh x - \sin x \cosh x = 0 \tag{2.12}$$

For each eigenvalue $\lambda_n = \mu_n^4$ there is, from equation (2.9), a ODE for $T(t)$

$$T''(t) + \omega_n^2 T(t) = 0, \quad \omega_n^2 = \lambda_n \frac{EI}{\rho A_0} \tag{2.13}$$

The general solution of equation (2.13) is $T_n(t) = \alpha_n \cos\omega_n t + \beta_n \sin\omega_n t$. Superposition principle gives the solution to equation (2.8) as $w(x,t) = \sum_{n=1}^{\infty} X_n(x)T_n(t)$ and the constants c_n, α_n and β_n is decided from initial conditions. From the roots $(\mu_n L)$ of equation (2.12) the eigenvalues λ_n, the eigenfunctions (mode functions) X_n and the eigenfrequencies (natural

frequencies) ω_n can be computed. The nodes for the eigenfunctions is given by solving $X_n(x) = 0$, node positions normalized by L for a fixed-pinned beam are shown in Table 2.1. The natural frequency in Hz in terms of $(\mu_n L)$ is given by equation (2.14). The first mode natural frequency is called the fundamental frequency and if this is known the higher mode frequencies can be computed from equation (2.15), which can easily be derived from (2.14).

$$f_n = \frac{\omega_n}{2\pi} = \frac{1}{2\pi}\frac{(\mu_n L)^2}{L^2}\sqrt{\frac{EI}{\rho A_0}} \tag{2.14}$$

$$f_n = f_1 \frac{K_n}{K_1}, \quad K_n = (\mu_n L)^2 \tag{2.15}$$

Table 2.1: Node positions normalized by L for the first 6 modes, $\mu_n L$ are solutions to equation (2.12) and $K_n = (\mu_n L)^2$ which appears in equation (2.14).

Mode	$\mu_n L$	K_n	Node positions/L					
1	3.927	15.418	0	1				
2	7.069	49.965	0	0.5575	1			
3	10.210	104.248	0	0.3860	0.6922	1		
4	13.352	178.270	0	0.2951	0.5294	0.7647	1	
5	16.493	272.031	0	0.2389	0.4285	0.6190	0.8095	1
6	19.635	385.531	0	0.2007	0.3600	0.5200	0.6800	0.8400	1

2.2 Fluid model

The method of solving problems involving fluid flow is called *computational fluid dynamics (CFD)*. The principle is similar to the FEM, the fluid volume is divided into small volumes, and the transport equations are solved for each volume. This is called the finite volume method (FVM). Different discretization schemes can be used to approximate the derivatives such as first or second order upwind, or central differencing. This leads to a system of equations, which usually must be solved iteratively. The steps in the discretization are to generate a grid, integrate the transport equations over the cell volumes and approximate the derivatives with some discretization scheme. The result is a discretized system of equations that gives an approximate solution of the flow variables when solved. [4]

2.2.1 Governing equations of fluid flow

The governing equations of fluid flow come from the principles of conservation of mass and momentum. Since the fluid in this problem is water, the flow is assumed to be incompressible. *The continuity equation* (2.16) is derived from the principle conservation of mass. Using the incompressibility assumption the continuity equation can be simplified as (2.17). *The momentum equation* is given by (2.18). [4]

$$\frac{\partial \rho}{\partial t} + \frac{\partial \rho v_i}{\partial x_i} = 0 \tag{2.16}$$

$$\frac{\partial v_i}{\partial x_i} = 0 \tag{2.17}$$

$$\frac{\partial \rho v_i}{\partial t} + \frac{\partial \rho v_i v_j}{\partial x_j} = -\frac{\partial p}{\partial x_i} + \frac{\partial \tau_{ij}}{\partial x_j} + \rho f_i \tag{2.18}$$

In momentum equation (2.18) one term includes the viscous stresses τ_{ij}. In a Newtonian fluid and for incompressible flow the viscous stresses will be on the following form. [5]

$$\tau_{ij} = \mu \left(\frac{\partial v_i}{\partial x_j} + \frac{\partial v_j}{\partial x_i} \right)$$

Inserting this expression for the stresses in momentum equation gives *the Navier-Sokes equation* (2.19) (the body forces ρf_i will be ignored in the continuing).

$$\frac{\partial \rho v_i}{\partial t} + \frac{\partial \rho v_i v_j}{\partial x_j} = -\frac{\partial p}{\partial x_i} + \frac{\partial}{\partial x_j} \left(\mu \left(\frac{\partial v_i}{\partial x_j} + \frac{\partial v_j}{\partial x_i} \right) \right) \tag{2.19}$$

Now there are four equations, (2.17) and (2.19) and four unknown p,v_i for $i = 1, 2, 3$.

2.2.2 Turbulence and turbulence modeling

There are different ways to model turbulence. In this section two different principles of turbulence modeling are presented.

Reynolds-averaged Navier-Stokes equations

For turbulent flows the variables can be divided into a time-averaged part $\bar{\phi}$ and a fluctuating part ϕ', called Reynolds decomposition.

$$\phi = \bar{\phi} + \phi'$$

The time-averaged part is independent of time, $\overline{\bar{\phi}} = \bar{\phi}$, and the fluctuating part has zero mean value, $\overline{\phi'} = 0$. For the velocity components and the pressure Reynolds decomposition gives the following expressions.

$$v_i = \bar{v}_i + v_i', \quad p = \bar{p} + p' \tag{2.20}$$

Insert the Reynolds decompositions (2.20) in continuity equation (2.17) and Navier-Stokes equation (2.19) for incompressible flow and take the time average of each equation gives the *Raynolds-averaged Navier-Stokes (RANS) equations* (2.21).

$$\frac{\partial \bar{v}_i}{\partial x_i} = 0 \tag{2.21a}$$

$$\rho \left(\frac{\partial \bar{v}_i}{\partial t} + \bar{v}_j \frac{\partial \bar{v}_i}{\partial x_j} \right) = -\frac{\partial \bar{p}}{\partial x_i} + \frac{\partial}{\partial x_j} \left(\mu \left(\frac{\partial \bar{v}_i}{\partial x_j} + \frac{\partial \bar{v}_j}{\partial x_i} \right) - \rho \overline{v_i' v_j'} \right) \tag{2.21b}$$

The last term $\rho \overline{v_i' v_j'}$ is called the turbulent stresses (or the Reynolds stresses) and can be modeled by Boussinesq assumption (2.22).

$$\rho \overline{v_i' v_j'} = -\mu_t \left(\frac{\partial \bar{v}_i}{\partial x_j} + \frac{\partial \bar{v}_j}{\partial x_i} \right) + \frac{2}{3} \delta_{ij} \rho k \tag{2.22}$$

Depending on the definition of time-average equation (2.21) can be steady or unsteady, then called the *unsteady Reynolds-averaged Navier-Stokes (URANS)*. The turbulent eddy viscosity μ_t is still unknown and can be modeled in different ways. Common models for the turbulent eddy viscosity are the $k-\varepsilon$ model and the $k-\omega$ model. In the $k-\varepsilon$ model transport equations is derived for the turbulent kinetic energy, k and its dissipation, ε. The turbulent viscosity is then expressed in the turbulent kinetic energy and the dissipation. The procedure for the $k-\omega$ model is the same, but the turbulent viscosity is instead expressed in k and the specific dissipation, ω, and transport equations must be derived for these quantities. [6]

Large eddy simulation

The principle in eddy simulation (LES) is to resolve the large eddies (grid scales) and model the small eddies (subgrid scales). In LES the continuity and Navier-Stokes equations is filtered (volume-averaged) instead of time averaged as in the RANS. The variables are split up as $\phi = \bar{\phi} + \phi''$ and for volume averaging $\bar{\phi} \neq \overline{\bar{\phi}}$ and $\overline{\phi''} \neq 0$. The governing equations for LES is described in equation (2.23).

$$\frac{\partial \bar{v}_i}{\partial x_i} = 0 \tag{2.23a}$$

$$\rho\left(\frac{\partial \bar{v}_i}{\partial t} + \bar{v}_j\frac{\partial \bar{v}_i}{\partial x_j}\right) = -\frac{\partial \bar{p}}{\partial x_i} + \frac{\partial}{\partial x_j}\left(\mu\left(\frac{\partial \bar{v}_i}{\partial x_j} + \frac{\partial \bar{v}_j}{\partial x_i}\right) - \rho(\overline{v_i v_j} - \bar{v}_i\bar{v}_j)\right) \tag{2.23b}$$

A subgrid model is needed to model she subgrid-scale stresses, $\tau_{ij} = \rho(\overline{v_i v_j} - \bar{v}_i\bar{v}_j)$. There are different subgrid scale models, for example Smagorinsky model and Wall-Adapting Local Eddy-viscosity (WALE) model, both using the Boussinesq assumption (2.22) and models the turbulent eddy viscosity, ν_t. [6]

2.3 Fluid structure interaction

In problems with fluid-structure interaction (FSI) solid structures interact with surrounding fluid flow. The solid structure displacement will cause pressure differences in the fluid, and these pressure differences will force, or damp, the motion of the structure. One example of this phenomena is when turbulence in the flow cause motion of some structure, this is called *flow induced vibrations*. There are different numerical methods for solve these types of problems. The *monolithic* approach solves the fluid and structure dynamics as one system of equations, this method require conforming mesh and a specialized code. The *partitioned* approach solves the fluid and structure system separately with different meshes and codes. The advantage with this approach is that common and well known codes can be used and connected together. [7]

The partitioned approach is the method used in the simulations in this thesis, connecting ANSYS Mechanical with ANSYS Fluent. A partitioned FSI simulation can also be *one-way* or *two-way* coupled. In a one-way coupled simulation data is only transferred from one solver to the other, but not the opposite way. In two-way coupled FSI both part is affected by each other and data is transferred both from fluid solver to structure solver and from structure solver to fluid solver.

2.4 The software

The software used for the simulations is ANSYS Mechanical and ANSYS Fluent coupled together via System coupling application in ANSYS Workbench. The structure model is set up in Mechanical, including boundary conditions. The surfaces which are in contact with the fluid get a special FSI-condition. The fluid model and solver settings are set up in Fluent, and also here the surfaces in contact with the moving structure is set as "FSI-walls". The data transfers between the fluid solver (Fluent) and the structure solver (Mechanical) are defined in the System coupling application. During the solution process, the displacements calculated in Mechanical are transferred to Fluent FSI-wall, and the pressure calculated in Fluent is transferred to Mechanical FSI-surface. During a time step data is transferred between the solvers multiple times, until some convergence criteria (or maximum number of iterations) is reached. In System coupling the end time, time step and maximum number of iterations in each time step is defined. A flow chart of the FSI workflow in ANSYS is shown in Figure 2.1. [8]

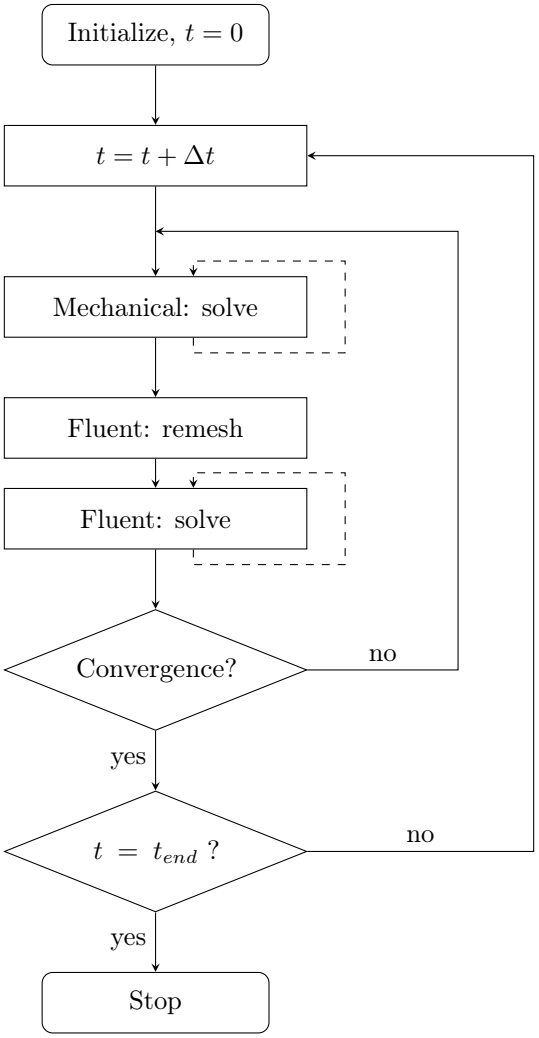

Figure 2.1: *Flow chart for two-way coupled FSI with ANSYS Workbench.*

There could be convergence problem for these types of simulations. In ANSYS there is

a special *Solution stabilization* parameter implemented to stabilize the computations. This parameter is modifying a coefficient in the discretized continuity equation to slow down the pressure response in the fluid when a displacement from the mechanical solver is received. Before taking the next time step the structure displacement and the fluid pressure should have converged, hence the pressure difference between the coupling iterations is zero. This method will avoid divergence or oscillating around the solution and affect the rate of convergence. The converged solution will not be affected. [9]

2.5 Frequency analysis

To analyze the frequency content in vibration data the Discrete Fourier Transform (DFT) is used. The DFT transform some discrete data from time-domain into discrete data in frequency domain. The DFT of some data $\{x_n\}_{n=0}^{N}$ with length N is

$$X_k = \frac{1}{N} \sum_{n=0}^{N-1} e^{-nk\frac{2\pi}{N}i} x_n. \tag{2.24}$$

The generated sequence X_k will be periodic with period N, and symmetric around $k = 0$. The frequencies and its corresponding amplitude are calculated as

$$f_k = \frac{k}{\Delta t N}, \quad A_k = 2|X_k|, \quad 0 < k < N/2 \tag{2.25}$$

where Δt is the time step size of the sample data. [10, 11]

3 Methodology

In this chapter the simulation set up and model is described. First the geometry, the computational domain and the material properties are explained in section 3.1. Then in section 3.2 the case set up is presented and motivated.

3.1 The model

The geometry and the computational domain is built up with the same dimensions as the experiment described in section 1.1. The solid geometry consists of a long slender tube representing the neutron flux detector guide tube. The fluid domain around the tube represents the space between the fuel bundles. The neutron flux detector guide tube and the fuel bundles are also described in section 1.1. As shown in Figure 3.1 the length of the tube is 1486 mm, the outer diameter is 8 mm and the wall thickness is 0.6 mm. It is fixed at its lower end ($z = 0$ m) and pinned at its upper end ($z = 1.476$ m).

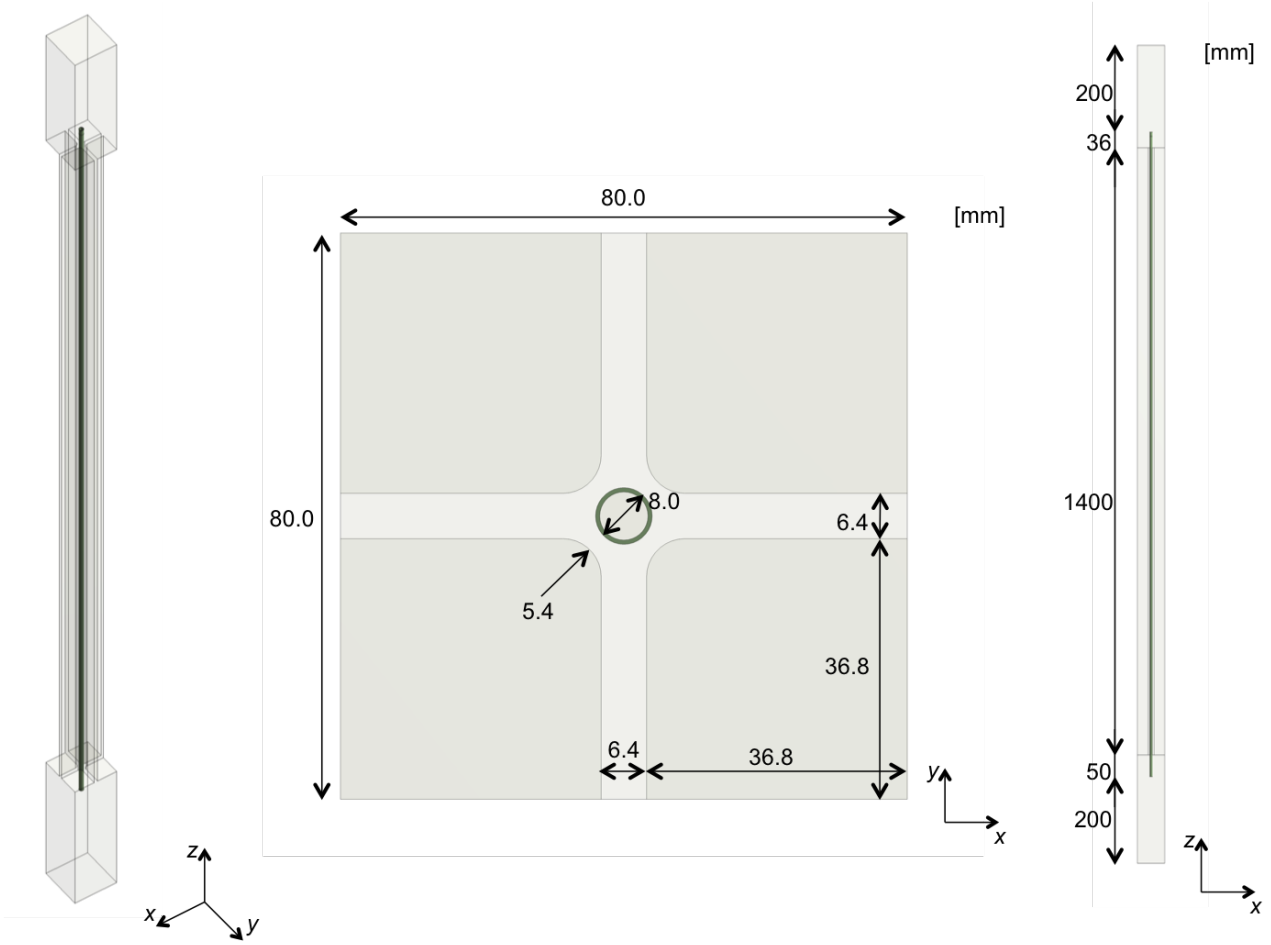

Figure 3.1: *Different views of the geometry and the computational domain. To the left there is a isometric view, in the middle the geometry is seen from above and to the right the geometry is seen from the side.*

The upper boundary condition is set 1 cm down from the end of the tube, and is modelled by setting x- and y-displacement to zero. At the inlet the mass flow is given and at the outlet the gauge pressure is 0 Pa. The tube is made of steel and the density used in the simulations is the same as in the experiment. The Young's modulus has been calibrated in order to obtain the same fundamental frequency for the tube in air as in the experiment. The material data used in the simulation is listed in Table 3.1 and Table 3.2.

Table 3.1: Material data for steel, used in the simulations.

Material	**Density [kg/m^3]**	**Young's modulus [GPa]**	**Poison's ratio**
Steel	7863	193	0.3

Table 3.2: Material data for air and water, used in the simulations [12].

Material	**Density [kg/m^3]**	**Dynamic viscosity [m^2/s]**	**Speed of sound [m/s]**
Air	1.2	$17.83 \cdot 10^{-6}$	343
Water	998.2	$1.002 \cdot 10^{-3}$	1497

3.2 Case set up

A modal analysis for the tube is done in ANSYS, in order to determine the eigenfrequencies and its mode shapes. The modal analysis is performed both in air and in water and the boundary condition used is fixed-pinned. The FSI-simulation is done for three different mass flow rates at the inlet, 5 kg/s, 10 kg/s and 14.8 kg/s. For mass flow rate 10 kg/s different turbulence models is tested in order to find out if there is any differences between the models. As it turned out that the URANS-models could not induce any vibration of the rod (see section 5.4) the LES-model is used most simulation.

Simulations is done using four different fluid meshes, a coarse mesh with 250 000 cells, a medium mesh of 1 million cells, a fine mesh of 2.5 million cells and one extra fine mesh with 10 million cells. The biggest difference between the meshes is in the "cross" around the tube, pictures of the meshes in the "cross"-part can be seen in appendix B. The coarse mesh was designed to run "fast" on the workstation for the purpose to find a working simulation set up and flow model. For this mesh the different turbulence model was tested in order to decide which model to use for the finer meshes. Also different inlet mass flows were tested for this mesh, to see if and how the flow rate affects the rod vibration. For the medium and fine mesh the case 10 kg/s is tested with LES. For the medium mesh the cell size around the tube is $\Delta x^+ \approx 1650$, $\Delta y^+ \approx 150$ and $\Delta z^+ \approx 170$. The fine mesh cells size around the tube is $\Delta x^+ \approx 1100$, $\Delta y^+ \approx 110$ and $\Delta z^+ \approx 90$. Since the amplitudes seemed to be a bit large (see chapter 5), two cases were run with 5% damping implemented in the structure model to see how much impact this could have on the vibration amplitude. The extra fine mesh was designed to test the computational time on a cluster. This mesh was run for one case, 10 kg/s and LES. It is used as verification and to test convergence sensitivity. For this mesh the cell

size is $\Delta x^+ \approx 820$, $\Delta y^+ \approx 80$ and $\Delta z^+ \approx 115$. For each mesh and flow rate the time step is adapted to get a desired Courant number for the simulation. The Courant number is kept around 5 in some simulations and around 1 in some simulations. Running the simulations for the finer meshes with Courant number around 1 requires small time step size which make the simulation very time consuming, hence it is interesting to see if a greater time step will affect the result.

Table 3.3: Cases simulated.

Mesh	**Mass flow [kg/s]**	**Turbulence model**	**Time step [ms]**	
coarse	5	LES	1.0	
coarse	10	LES	1.0, 0.5	
coarse	15	LES	0.25	
medium	10	LES	1.0, 0.2	
medium	10	LES	1.0, 0.2	damped
fine	10	LES	0.5, 0.15	
fine	10	LES	0.5, 0.15	damped
extra fine	10	LES	0.5	
coarse	10	URANS	1.0	
fine	10	URANS	0.5	

4 Experiment results

In this chapter the result of the experiments is presented. The displacements are measured at a position 850 mm from the bottom of the tube, normalized by the tube length it is 0.5720. This value is close to the node positions for the second mode at 0.5575 and the fourth mode at 0.5294 in Table 2.1, which means that in the frequency analysis almost nothing will be seen from the second and fourth mode. The sample frequency is 750 frames per second and hence frequencies up to 375 Hz could be resolved. For all trials the sample length is 20 seconds. The experiment is done for five different mass flow rates between 0-15 kg/s, but only result for 5, 10 and 15 kg/s is presented since only these flows are relevant for comparison with the simulations. Several trials are done for each flow rate but in some trials there were problem with the measuring equipment. In Table 4.1 displacement data from all trials of 5kg/s, 10 kg/s and 15 kg/s is shown. The graphics in Figure 4.2 and Figure 4.1 is data from case 1, 4 and 6 is shown but any case could be used because the data for the cases look all similar. The amplitude increases when the flow rate increases, which can be seen in Figure 4.1 showing the time-position data for the different flow rates.

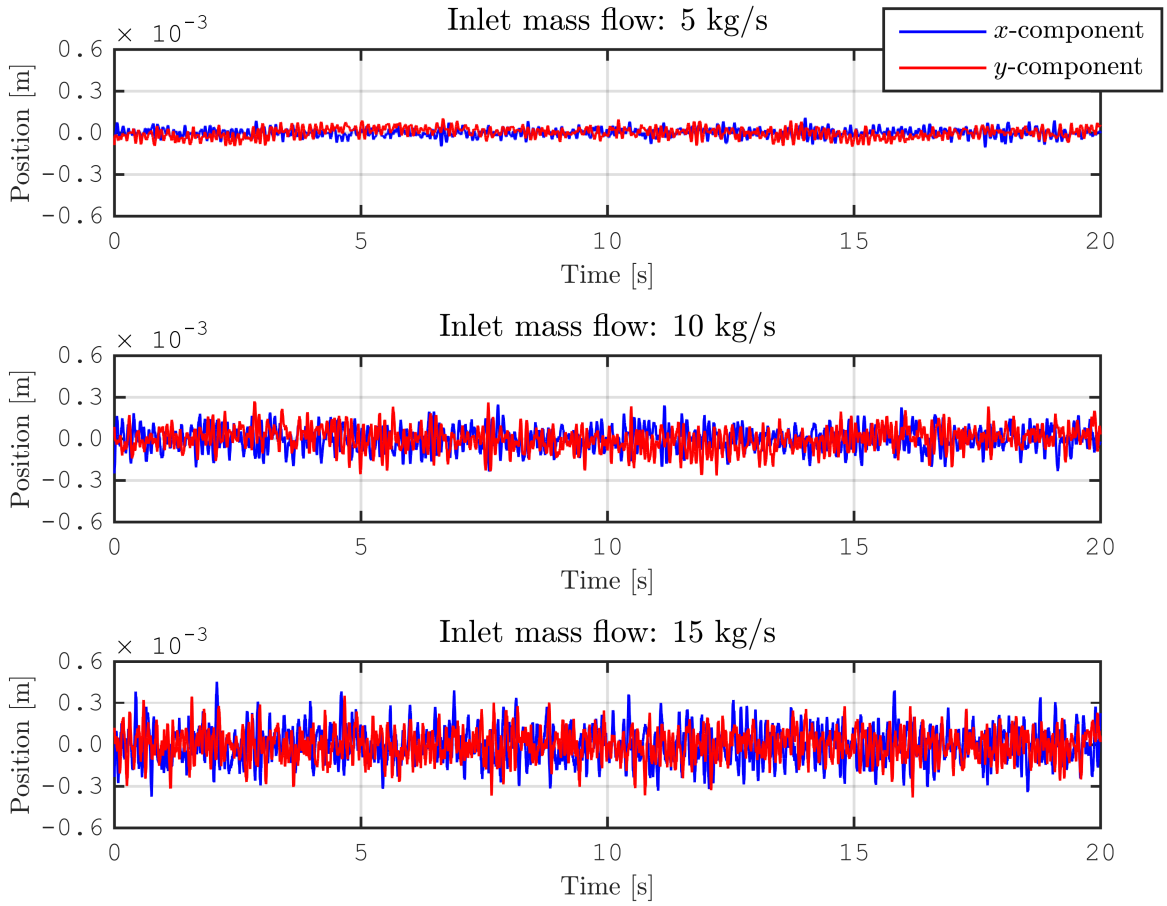

Figure 4.1: *Time-position data of the tube displacement for the different flow rates.*

Table 4.1: RMS-values and maximum values of tube displacement experiment data.

Case	Mass flow [kg/s]	Displacement [mm]					
		x-component		y-component		total	
		RMS	Max	RMS	Max	RMS	Max
1	**5**	0.0286	0.1084	0.0356	0.1039	0.0457	0.1168
2	**5**	0.0323	0.1409	0.0316	0.1326	0.0452	0.1897
3	**10**	0.0786	0.2562	0.0798	0.3268	0.1120	0.3279
4	**10**	0.0780	0.2494	0.0802	0.2705	0.1118	0.3074
5	**10**	0.0755	0.2847	0.0702	0.2713	0.1031	0.3921
6	**15**	0.1238	0.4550	0.1050	0.3802	0.1623	0.4557
7	**15**	0.1249	0.4962	0.1106	0.4056	0.1668	0.5137

The fundamental frequency of the tube is determined by measurements when the tube is bent out and released, in both air and still water. The results are presented in Table 4.2. Using equation (2.15) and data in Table 2.1 the higher modes can be estimated, which are presented in Table 4.3.

Table 4.2: Fundamental frequencies for the tube from experimental tests.

Mode	Air [Hz]	Water [Hz]
1	14.65	10.25

Table 4.3: Estimations of higher modes using the first mode frequencies in Table 4.2.

Mode	K_n	Frequency [Hz], $f_n = f_1(K_n/K_1)$	
1	15.418	14.65	10.25
2	49.965	47.47	33.21
3	104.248	99.03	69.29
4	178.270	169.35	118.49
5	272.031	258.43	180.81
6	385.531	366.25	256.25

The frequency content from vibration (displacement) data is shown in Figure 4.2. The peaks in Figure 4.2 are located around 10 Hz, 65 Hz, 152 Hz and 170 Hz, where 10 Hz and 65 Hz match with the first and third mode in Table 4.3. As expected the second and forth mode cannot be found in the frequency spectra. The fifth mode frequency is 180 Hz according to the estimates in Table 4.3 and there is one peak on 170 Hz in Figure 4.2 that match this mode, but there is also one peak at 152 Hz which does not have a clear match with any of the estimated values.

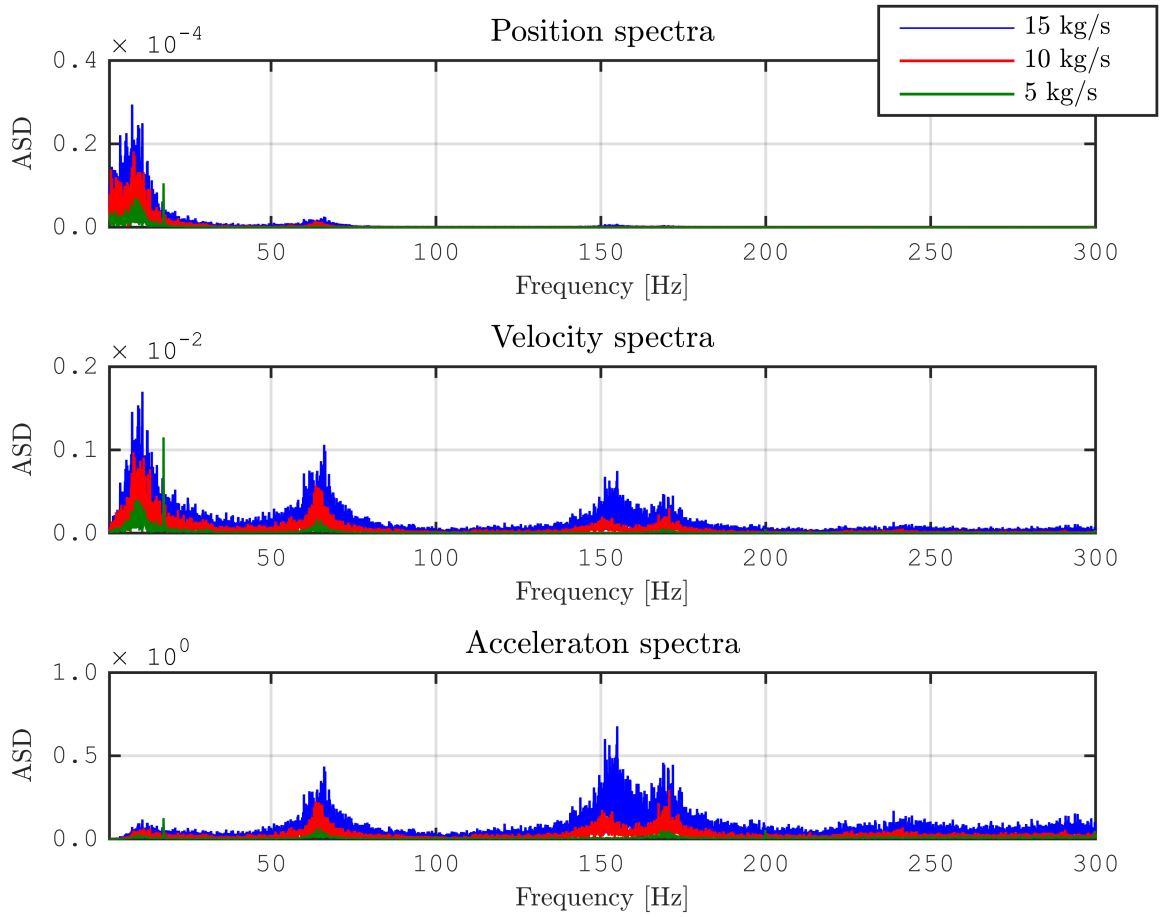

Figure 4.2: *Amplitude spectra for position, velocity and acceleration of the tube displacement for the different flows rates.*

5 Simulation results

In this chapter the results from the different simulations is presented. The result is mainly presented as x- and y-displacement of the tube in one point. The displacement is measured in a point 1118 mm from the bottom of the tube for the coarse mesh and 950 mm from the bottom of the tube for the other meshes. The frequency content and RMS-value of the displacement data are used to analyze and compare the simulations to each other and to the experiment data. The bulk velocity in the "cross"-channel is 5.23 m/s, 10.46 m/s and 15.69 m/s for inlet mass flow 5 kg/s, 10 kg/s and 15 kg/s respectively. In all results up to section 5.4 LES is used in the simulations.

5.1 Modal analysis

Table 5.1 shows the result of the modal analysis in ANSYS Mechanical. Estimation of the modes using equation (2.15) is given in Table 5.2. The fundamental frequency in air is the same as in the experiment since the Young's modulus is calibrated to obtain this frequency. The frequencies in water are higher in the simulation compared to the experiment, but it matches well with the estimations in Table 5.2.

Table 5.1: Modes computed in ANSYS Mechanical.

Mode	**Air [Hz]**	**Water [Hz]**
1	14.65	12.15
2	47.45	39.35
3	98.94	82.07

Table 5.2: Estimations of the modes using the first mode frequencies in tabel.

Mode	K_n	**Frequency [Hz],** $f_n = f_1(K_n/K_1)$	
1	15.418	14.65	12.15
2	49.965	47.47	39.37
3	104.248	99.03	82.13
4	178.270	169.35	140.45
5	272.031	258.43	214.33
6	385.531	366.25	303.75

5.2 Different mass flow rates

The tube vibration is simulated for three different inlet mass flows for the coarse mesh, the x- and y-displacement for these simulations are shown in Figure 5.1. It is clear from the figure that the vibration amplitude increases with the mass flow. In Table 5.3 the RMS-value and max-values of the displacement data are shown. The RMS-values of total displacement is about twice as big for these simulations compared to the experiments. For these three simulations

the time step is chosen so that the Courant number is around one. The time simulated is 3 seconds for case 1, 4.3 seconds for case 2 and 2 seconds for case 3. The frequency content in displacement data for simulation case 1, 2 and 3 is shown in Figure 5.2. The peaks in Figure 5.2 appear at 11 Hz, 37 Hz, 126 Hz, 200 Hz and 277 Hz. The frequencies in the simulations match well with the estimated frequencies in Table 5.2, but the third mode is missing in the simulation data as expected (since the normalized position is 0.75, close to the fourth mode according to Table 2.1). Separate graphs for each mass flow of the frequency content can be found in Appendix D.

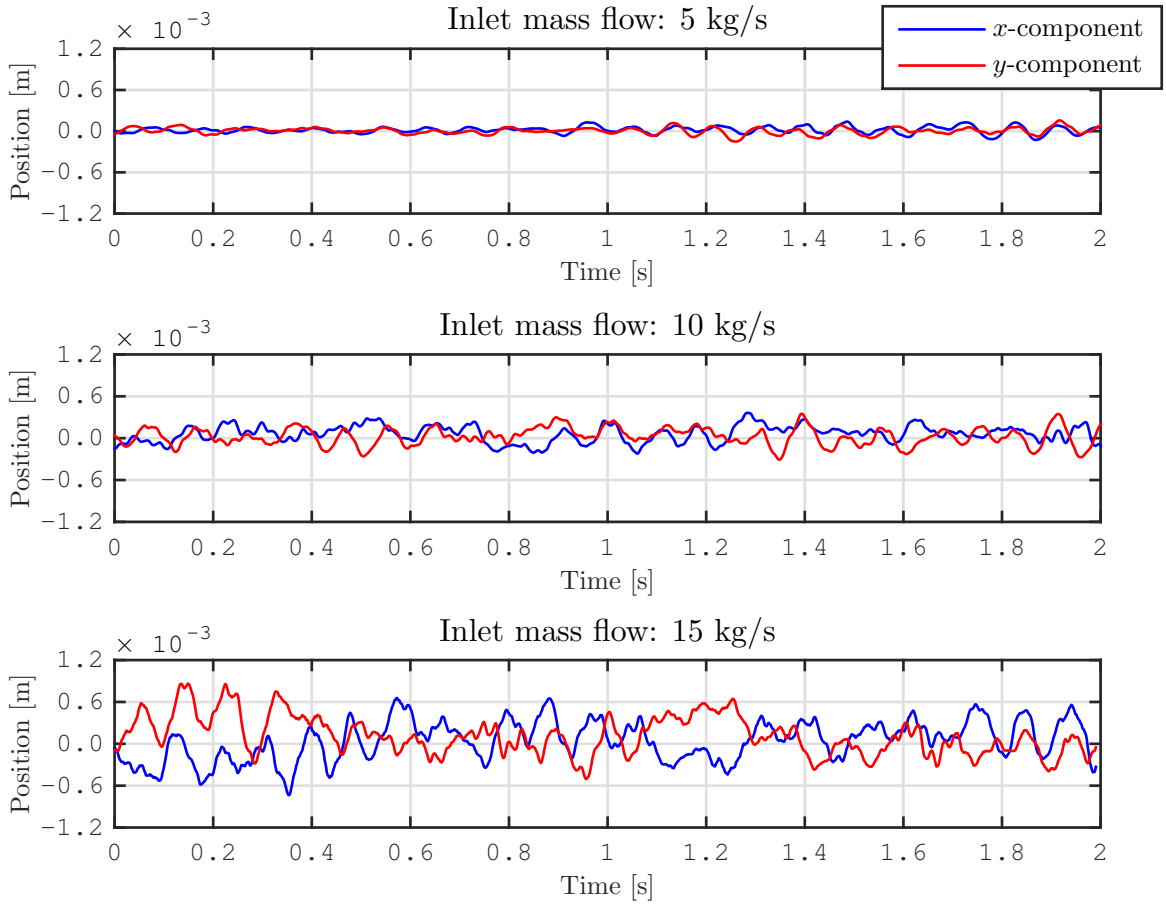

Figure 5.1: *Displacement of the tube for the different flows.*

Table 5.3: RMS-values and maximum values of tube displacement.

Case	Mass flow [kg/s]	Time step [s]	Displacement [mm]					
			x-component		y-component		total	
			RMS	Max	RMS	Max	RMS	Max
1	**5**	**0.001**	0.05	0.14	0.05	0.16	0.07	0.18
2	**10**	**0.0005**	0.14	0.36	0.13	0.38	0.19	0.44
3	**15**	**0.00025**	0.29	0.74	0.30	0.86	0.41	0.90

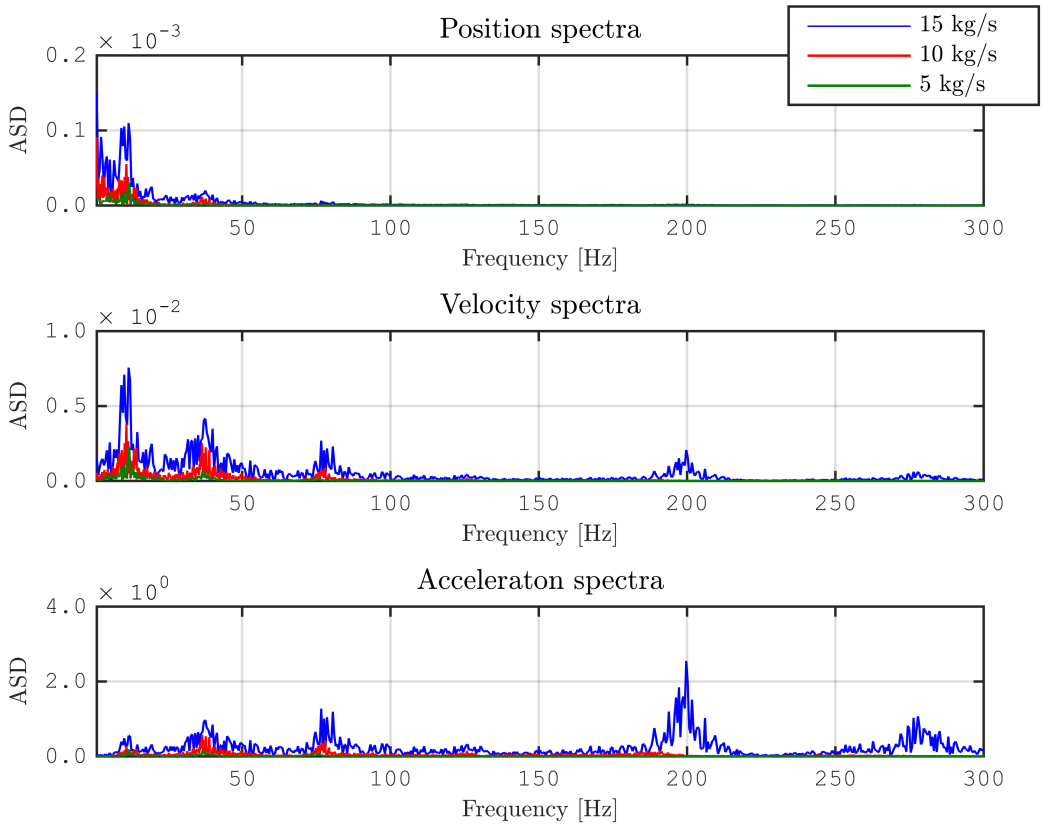

Figure 5.2: *Amplitude spectra for position, velocity and acceleration of the tube displacement.*

5.3 Sensitivity and convergence analysis

For the inlet mass flow 10 kg/s simulations are done with different meshes and time steps. In Table 5.4 information for all simulations for 10 kg/s is presented, in Appendix C the same table with RMS- and max-values for x- and y-components can be seen. The amplitude seems to be twice as large for the medium mesh (2) and fine mesh (3) compared to the coarse mesh (1) comparing RMS-values. For mesh 4 (finest mesh) the amplitude is a little lower compared to mesh 2 and mesh 3. Smaller time steps (Courant numbers around 1 instead of 5) do not seem to have any affect on the amplitudes, in some simulations the amplitude increases when the time step is decreased, and in some simulation the amplitudes decreases when the time step is decreased. Unfortunately the time simulated for the smaller time steps is short, less than one second in some cases. This is because of the computational cost when decreasing the time step, these simulations took over one week to run. Because of the large amplitudes compared to the experiment some simulations were run with 5 % structural damping implemented in ANSYS Mechanical, as described in section 3.2. The damping did not seem to decrease the amplitude. The mesh, time step and damping had no effect on the frequency content. Figure 5.3 shows the frequency content for simulation with the finest mesh. Since the displacement measurement point were at 950 mm from the bottom of the tube (0.64 when normalized with tube length) even the fourth mode frequency can be seen here.

Table 5.4: RMS-values and maximum values of tube displacement, Mesh 1 is the coarse mesh, Mesh 2 is the medium mesh, Mesh 3 is the fine mesh and Mesh 4 is the extra fine mesh.

Case	Mesh	Mass flow [kg/s]	Time step [s]	Time simulated [s]	Total displacement [mm]		
					RMS	Max	
2	1	10	0.0005	4.3	0.1927	0.4352	
4	1	10	0.001	3.5	0.1673	0.4094	
5	1	10	0.001	4.3	0.1708	0.4770	
6	2	10	0.001	1.1	0.3183	0.7303	
7	2	10	0.001	0.8	0.3474	0.6056	
8	2	10	0.0002	0.3	0.4069	0.9517	
9	2	10	0.001	0.8	0.3376	0.7417	Damped
10	2	10	0.0002	0.5	0.3748	0.7553	Damped
11	3	10	0.0005	1.7	0.3280	0.7443	
12	3	10	0.0005	1.4	0.4830	1.2180	Damped
13	3	10	0.00015	0.6	0.3239	0.7966	Damped
14	4	10	0.0005	1	0.2770	0.5505	

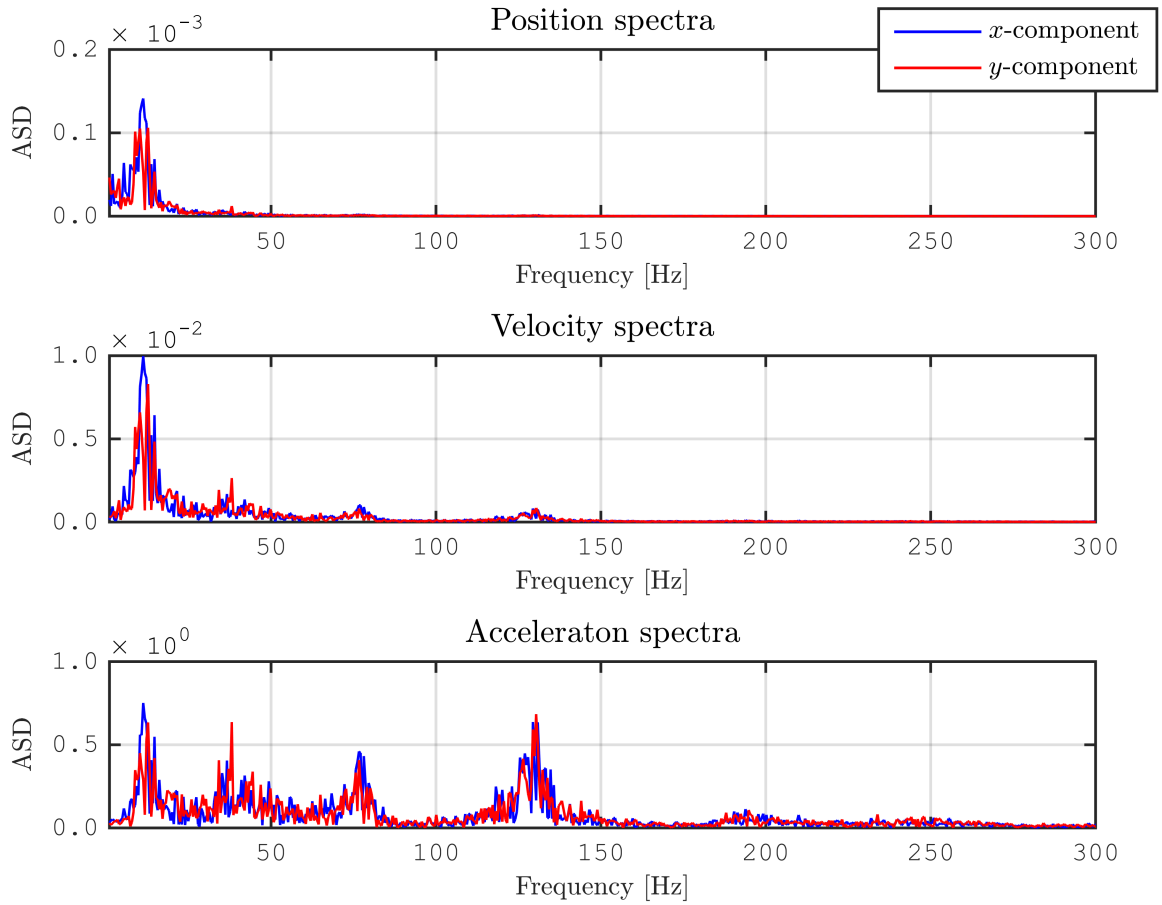

Figure 5.3: *Frequency content of vibrations for the extra fine mesh simulation.*

5.4 Different turbulence models

The URANS-models could not force any tube vibration. The upper graph in Figure 5.4 is an example of what happens when switching from LES to URANS SST-$k-\omega$ in Fluent. The flow then dampens the vibrations rather than inducing them. This simulation is done for the coarse mesh. The lower graph in Figure 5.4 shows a simulation switching from the $k-\varepsilon$-model to the SAS-model (a mix between URANS and LES), and then switching from the SAS-model to the LES. Clearly LES is the only of these modes that can induce the tube vibrations.

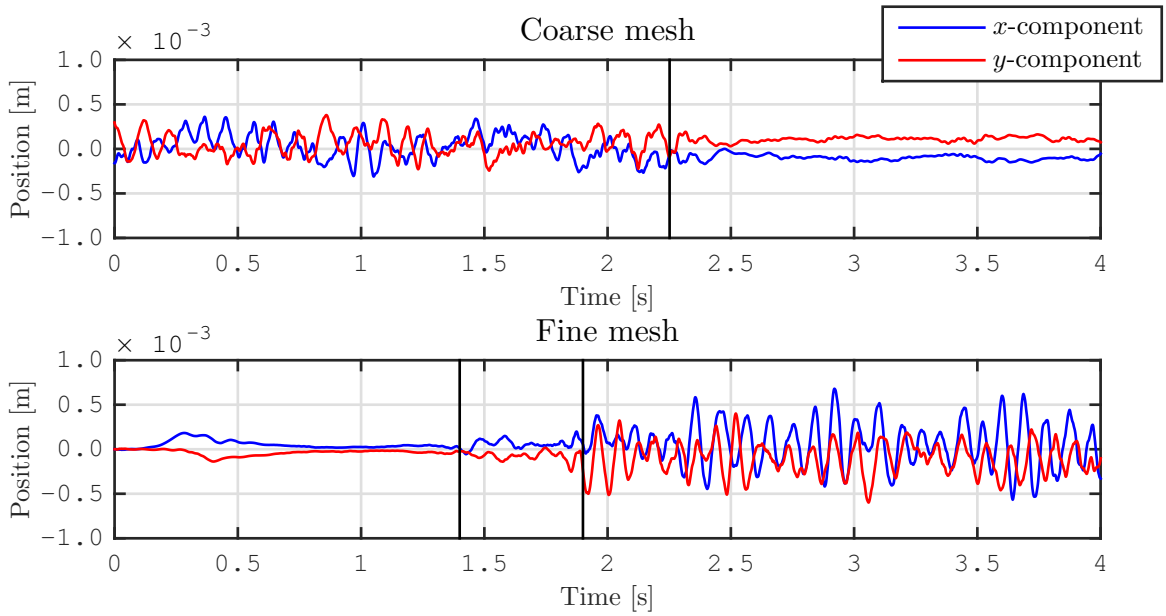

Figure 5.4: *Difference between the URANS model and the LES model.*

6 Discussion

When comparing the simulations to the experiment there were two things to notice. The amplitudes were far too high and the frequencies were a bit higher in the simulations compared to the experiment. The fundamental frequency in air was calibrated to be the same for the experiment and simulation. The Young's modulus was changed to get the right frequency in the simulation, since this parameter was unknown for the steel used in the experiment. It maybe would have been better to calibrate the frequency for water, but this were not done since it gave unreasonably low values of the Young's modulus. Hence there was already a gap between the frequencies in the experiment and the simulation before the FSI-simulation was performed. When doing a modal analysis in water in Mechanical the recommendation from ANSYS is to not have a to small volume of water around the object. In the experiments and the simulations the water channel around the tube is tight, which could possibly affect the frequencies. Also other parameters could be modified to calibrate the fundamental frequencies, for example the wall thickness of the tube or the distance between the boundary conditions, which were parameters with unknown tolerance. The difference in amplitude between the experiment and the simulation could be because of uncertainties in experiment set up or tolerances in the displacement measurements, but it is also possible that the simulation actually gives greater amplitudes. If this is always the case it would not be a big problem for industrial applications since the simulations then is conservative, the simulated case is worse than reality. The reason why the displacement is measured in different points in the simulation and the experiment is because of errors in the information and documentation of the experiment set up. This could be a reason to the difference in amplitude, but could not explain this big difference.

The amplitude is also larger for the finer mesh compared to the coarse mesh. This is probably because the turbulence, and the eddies is better resolved with the finer mesh. When analysing the flow it seems that a lot of turbulence is created in the inlet to the tight channel, but also from wall friction. Hence it is important to have a fine mesh around the tube wall. The simulations took long time, for the coarse mesh the simulations ran over a week on 4 cores to get around 4 seconds simulated. The simulations for the finest mesh also ran a week on 120 cores and only one second was simulated. For the finer mesh it was the re-meshing procedure in Fluent that was the most time consuming. This is the reason why not more time is simulated for the different cases, especially those cases with smaller time step. There were no problem with convergence, probably because of the very small deformations, hence solution stabilization was not needed for these simulations.

The LES could force vibrations, while the URANS could not. This is could be because a lot of turbulent viscosity is build up in the in the URANS-models. This turbulent viscosity will rather damp the tube vibrations than induce them.

7 Conclusions

It was possible to simulate the flow-induced vibrations of the tube with the LES. The differences in the frequency and amplitude could be because of differences in the model and the experiment. The simulations seemed not to be sensitive to time step or damping, but a coarse mesh resulted in lower amplitudes compared to a finer one.

7.1 Future work

Further benchmarking needs to be done to know that the simulation can be reliable. For this particular case it would be interesting to see similar results from other software. It would also be good to simulate longer time to get more robust data. Another area for further research is which turbulence models that can be used for this type of simulations, and why the models work or do not work. It could be interesting to investigate if it is the turbulence built up in the inlet or if it is the turbulence built up by shear along the walls that contributes most to the vibrations. It is also possible that a potential flow model can force tube vibrations, which could be interesting to investigate.

References

[1] Ottosen NS, Petersson H. *Introduction to the finite element method.* Harlow (UK): Pearson Education Limited, 1992.

[2] Sundström B, ed. *Handbok och formelsamling i hållfasthetlära.* Stockholm: Instutitionen för hållfasthetslära KTH, 1998.

[3] Ericsson F, Fant CH, Holmåker K. *Differentialekvationer och egenvärdesproblem.* Göteborg: Matematiska vetenskaper, CTH & GU, 2008.

[4] Versteeg HK, Malalasekera W. *An Introduction to Computational Fluid Dynamics: The finite volume method.* 2nd ed. Harlow (UK): Pearson Education Limited, 2007.

[5] White FM. *Fluid mechanics.* 7th ed. New York: McGraw Hill, 2011.

[6] Davidson L. *Fluid mechanics, turbulent flow and turbulence modeling.* Division of Fluid Dynamics, Department of Applied Mechanics, Chalmers University of Technology. 2015.

[7] Hou G, Wang J, Layton A. Numerical Methods for Fluid-Structure Interaction — A Review. *Commun. Comput. Phys.* **12**.2 (2012), 337–377.

[8] *System Coupling User's Guide.* ANSYS, Inc. 2015.

[9] *ANSYS Fluent User's Guide.* ANSYS, Inc. 2015.

[10] Råde L, Westergren B. *Matematics handbook for science and engineering.* Lund: Studentlitteratur, 2004.

[11] James G. *Advanced Modern Engineering Mathematics.* 2nd ed. Harlow (UK): Pearson Education Limited, 2011.

[12] Mörstedt SE, Hellsten G. *Data och diagram.* 7th ed. Stockholm: Liber AB, 2010.

A The test rig

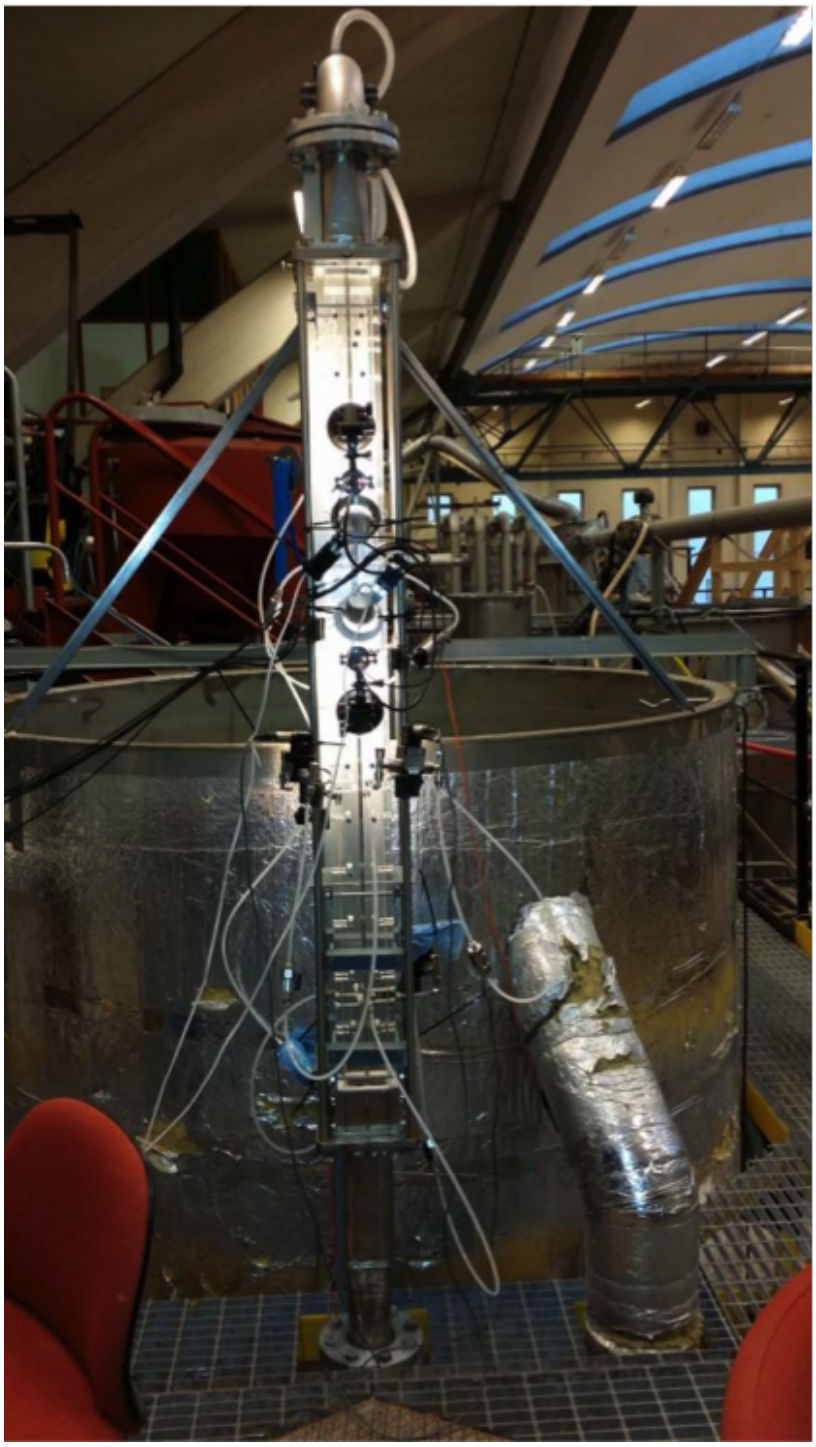

Figure A.1: *The rig used for the experiments.*

B Fluid meshes

B.1 Coarse mesh

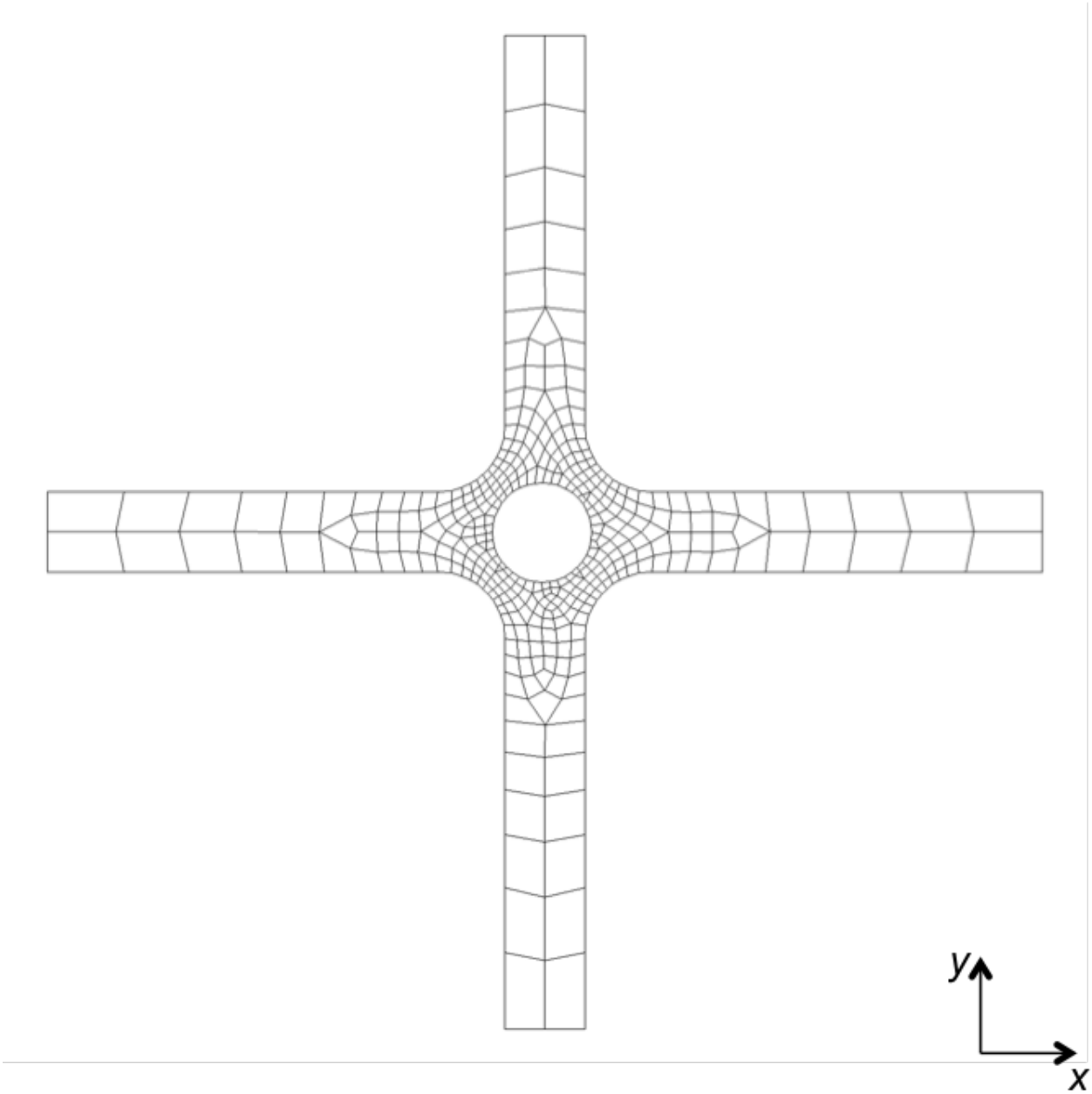

Figure B.1: *Coarse mesh.*

B.2 Medium mesh

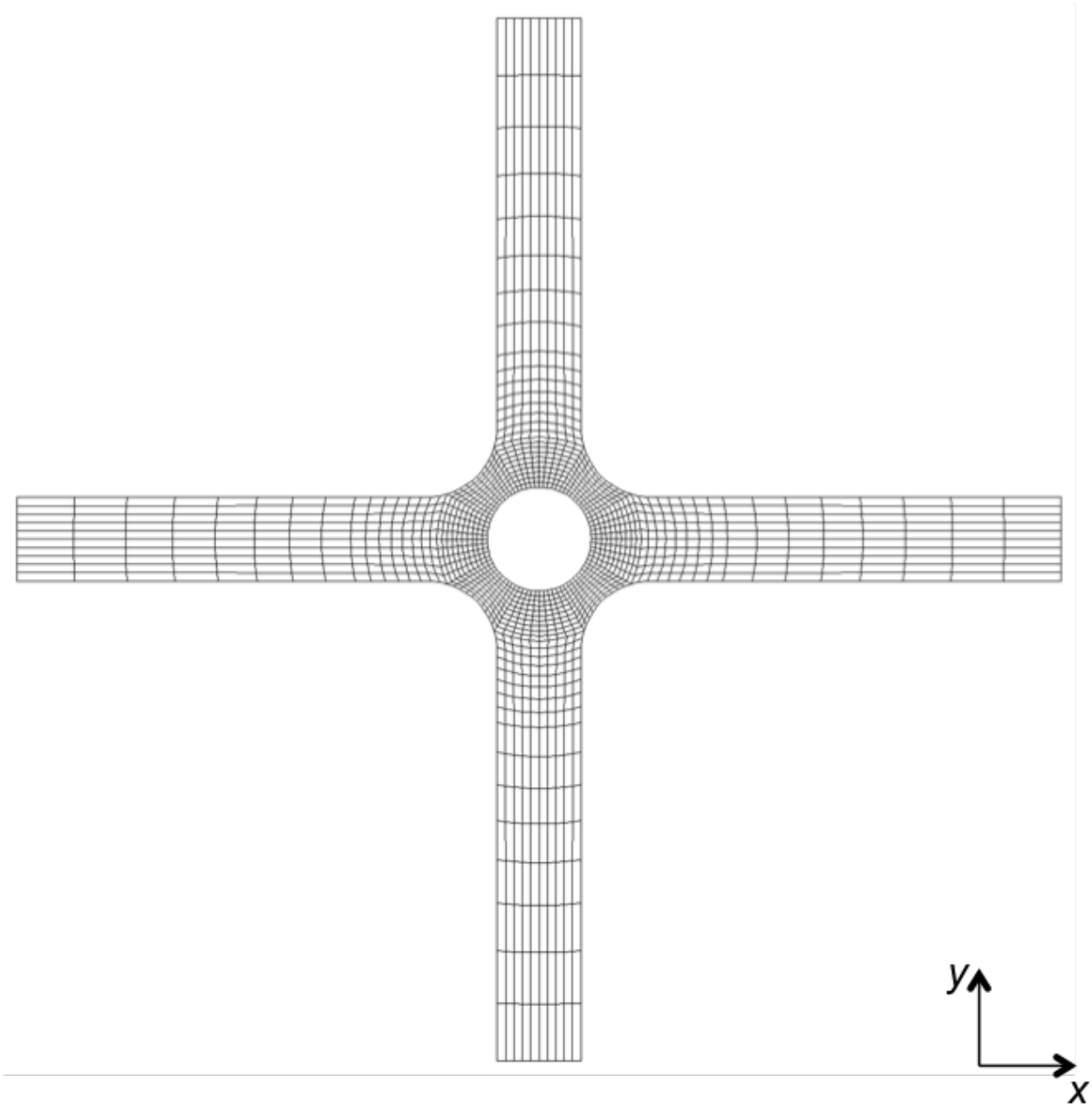

Figure B.2: *Medium mesh.*

B.3 Fine mesh

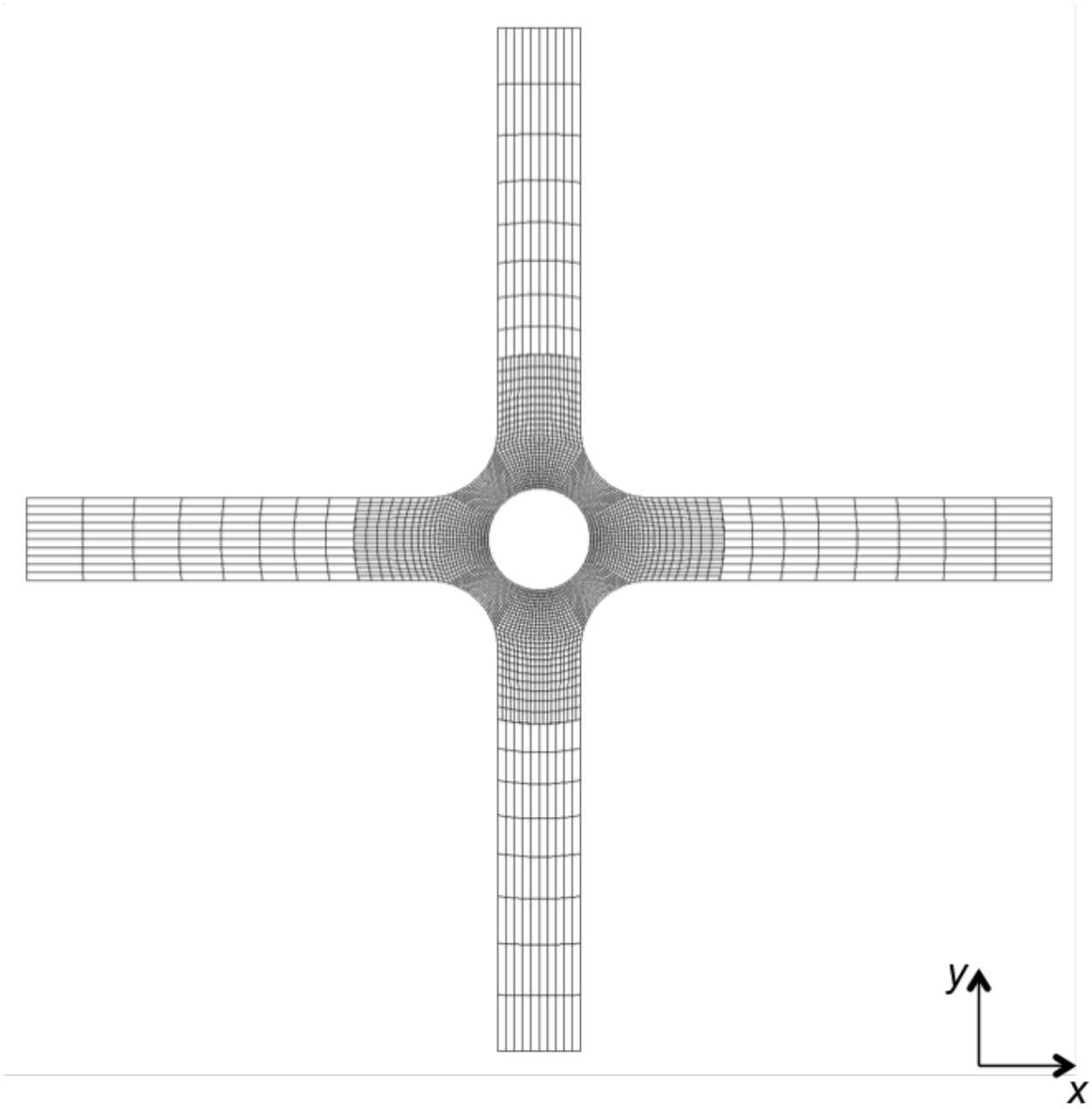

Figure B.3: *Fine mesh.*

B.4 Extra fine mesh

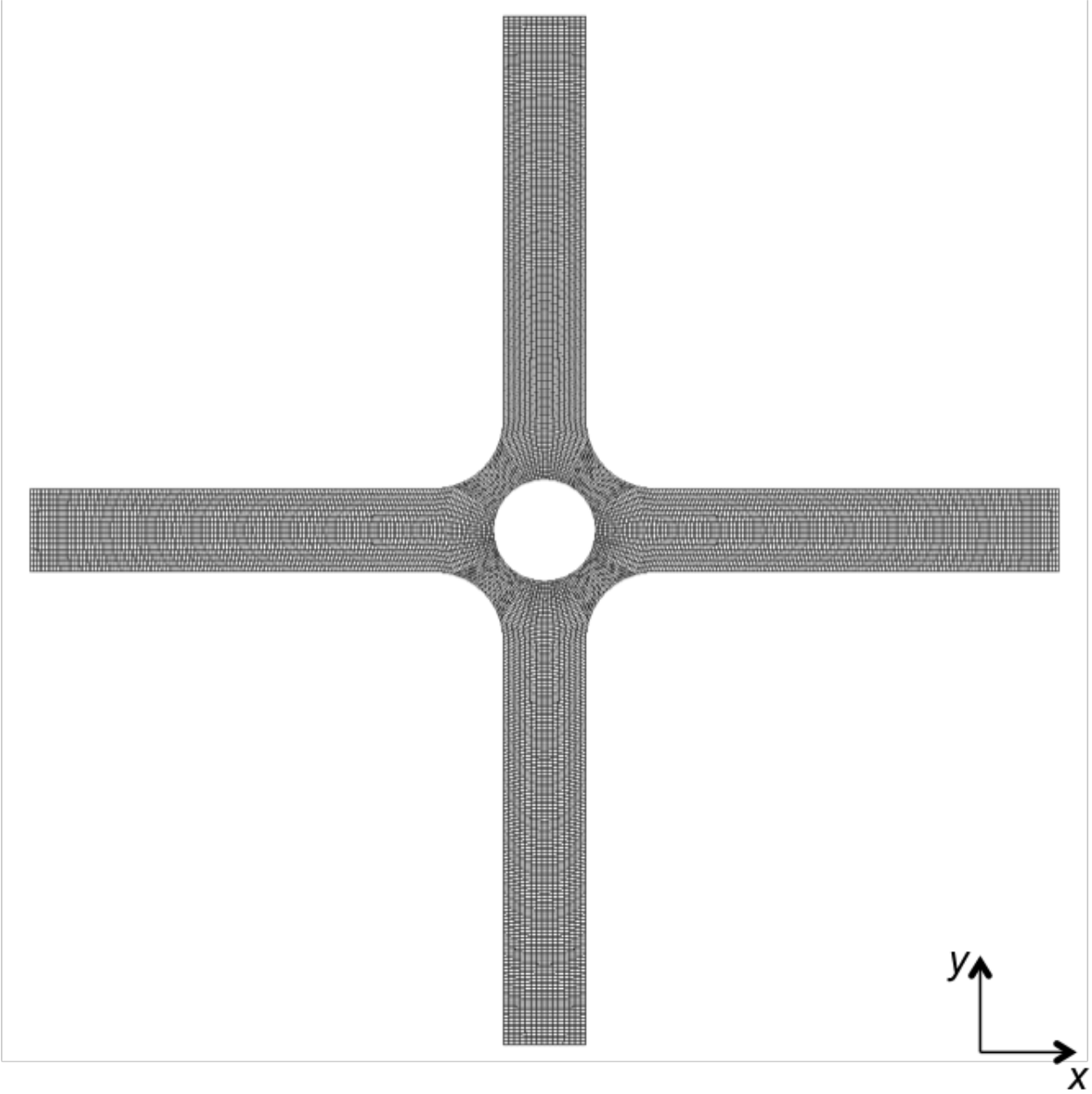

Figure B.4: *Extra fine mesh.*

C Displacement data

Table C.1: RMS-values and maximum values of tube displacement.

Case	Mesh	Mass flow [kg/s]	Time step [s]	Time simulated [s]	Displacement [mm]				Total		
					x-component		y-component				
					RMS	Max	RMS	Max	RMS	Max	
1	1	5	0.001	3	0.0482	0.1391	0.0459	0.1567	0.0666	0.1753	
2	1	10	0.0005	4.3	0.1395	0.3634	0.1329	0.3796	0.1927	0.4352	
3	1	15	0.00025	2	0.2861	0.7351	0.2980	0.8617	0.4131	0.9019	
4	1	10	0.001	3.5	0.1219	0.3839	0.1147	0.3001	0.1673	0.4094	
5	1	10	0.001	4.3	0.1238	0.4148	0.1177	0.3328	0.1708	0.4770	
6	2	10	0.001	1.1	0.2247	0.6595	0.2255	0.7246	0.3183	0.7303	
7	2	10	0.001	0.8	0.2526	0.5925	0.2385	0.5569	0.3474	0.6056	
8	2	10	0.0002	0.3	0.2781	0.7296	0.2971	0.6749	0.4069	0.9517	
9	2	10	0.001	0.8	0.2831	0.7379	0.1839	0.5004	0.3376	0.7417	Damped
10	2	10	0.0002	0.5	0.2703	0.5426	0.2597	0.6215	0.3748	0.7553	Damped
11	3	10	0.0005	1.7	0.2415	0.6789	0.2180	0.598	0.3280	0.7443	
12	3	10	0.0005	1.4	0.3225	0.9068	0.3595	1.2113	0.4830	1.2180	Damped
13	3	10	0.00015	0.6	0.2147	0.6454	0.2425	0.6028	0.3239	0.7966	Damped
14	4	10	0.0005	1	0.2117	0.5481	0.1787	0.5006	0.2770	0.5505	

D Ampltiude spectra for coarse mesh

D.1 Mass flow inlet 5 kg/s

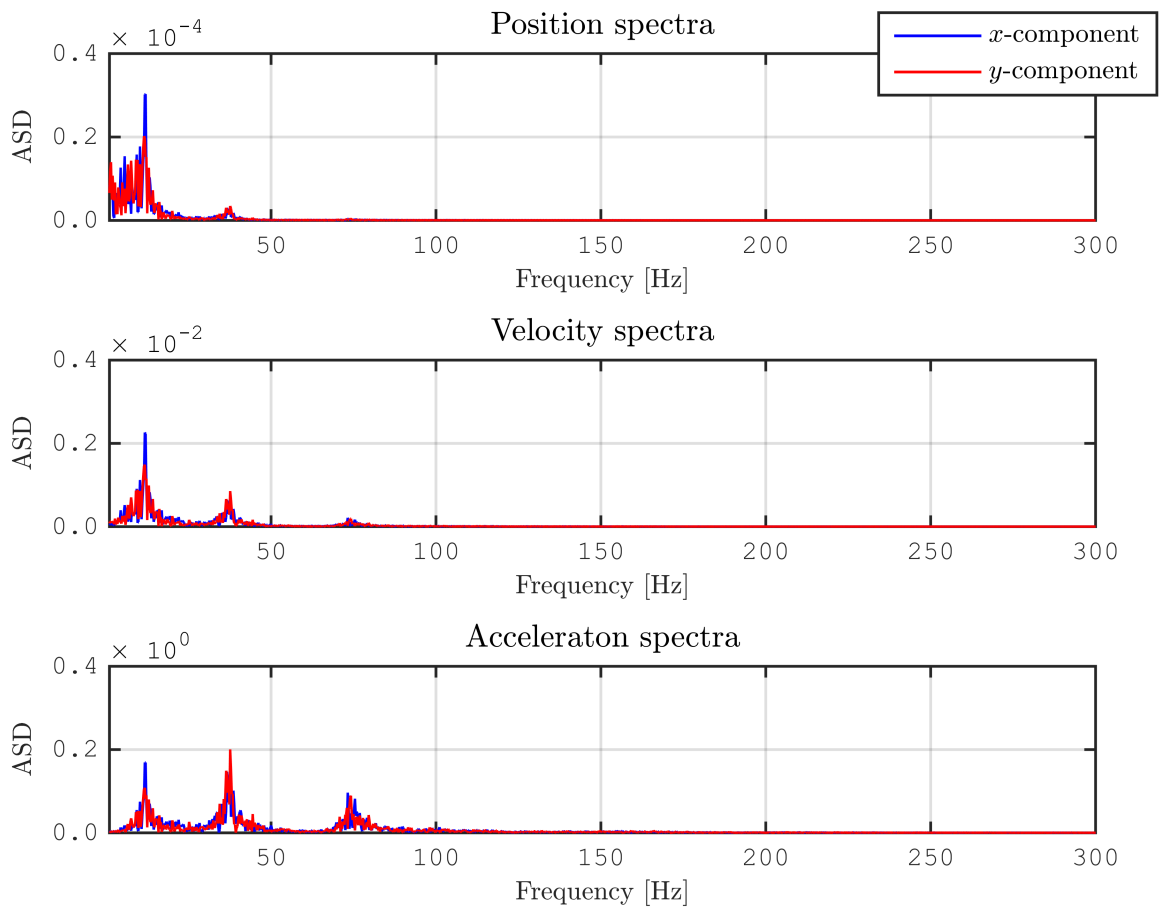

Figure D.1: *Frequncy content of vibrations for the 5 kg/s mass flow inlet simulation.*

D.2 Mass flow inlet 10 kg/s

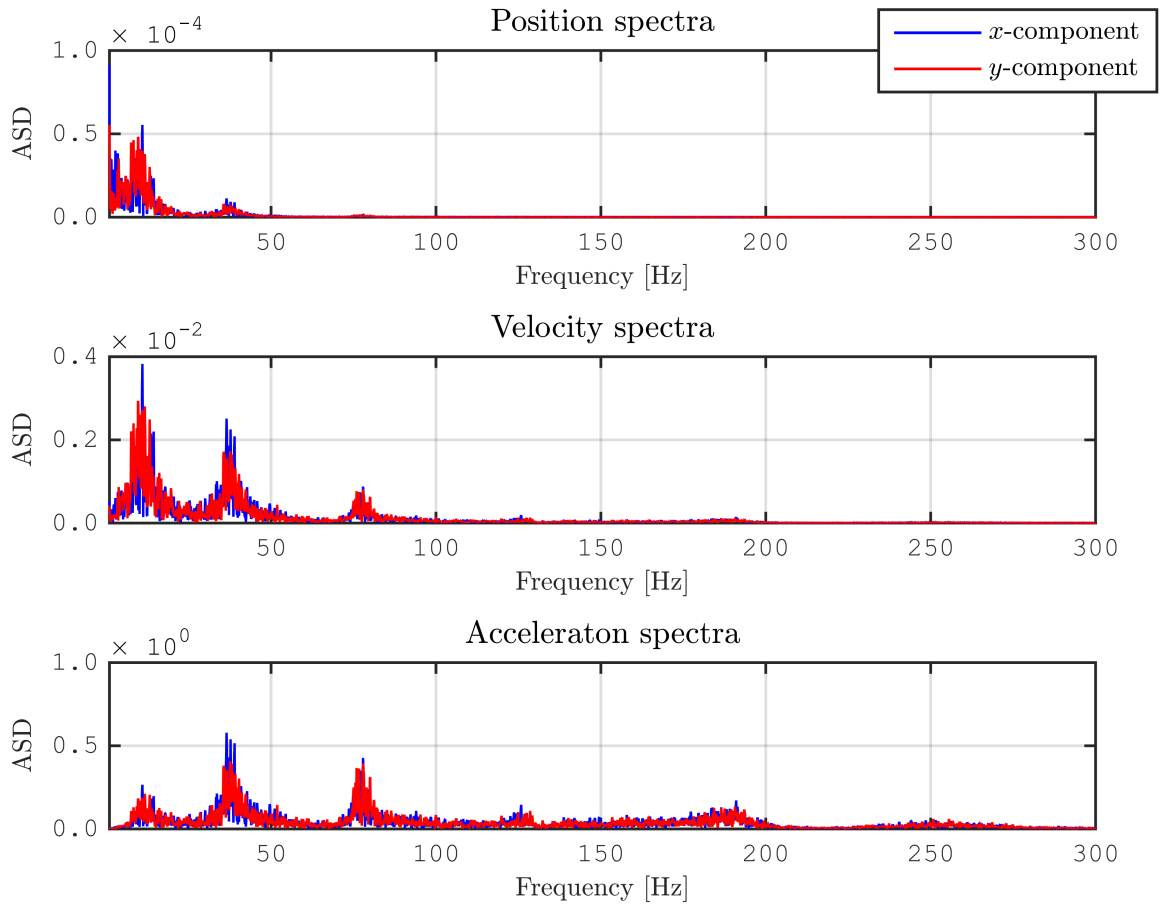

Figure D.2: *Frequncy content of vibrations for the 10 kg/s mass flow inlet simulation.*

D.3 Mass flow inlet 15 kg/s

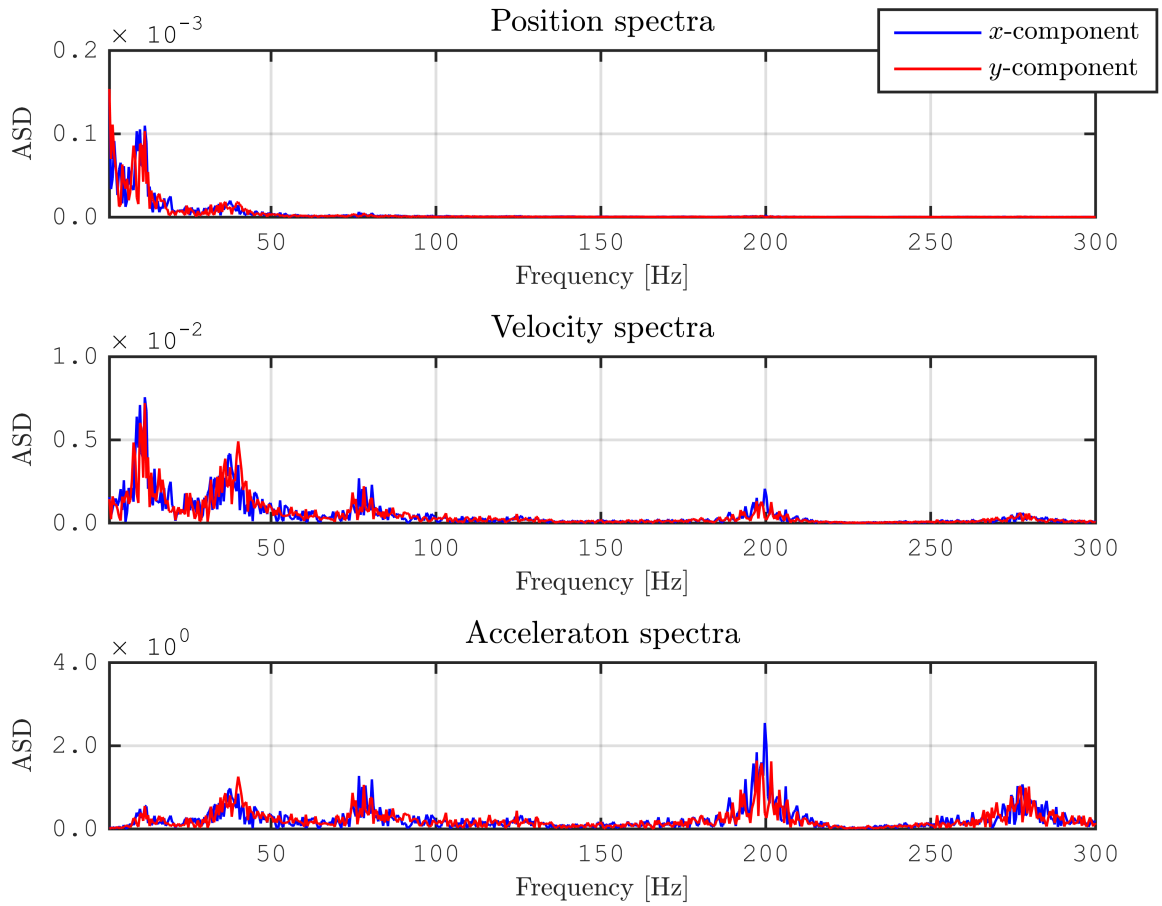

Figure D.3: *Frequncy content of vibrations for the 15 kg/s mass flow inlet simulation.*